

Three-dimensional weights of evidence modelling of a deep-seated porphyry Cu deposit



Ehsan Farahbakhsh¹, Ardesir Hezarkhani^{1*}, Taymour Eslamkish¹, Abbas Bahroudi² and Rohitash Chandra³

¹ Department of Mining Engineering, Amirkabir University of Technology (Tehran Polytechnic), Tehran, Iran

² School of Mining Engineering, College of Engineering, University of Tehran, Tehran, Iran

³ School of Mathematics and Statistics, University of New South Wales, Sydney, Australia

EF, 0000-0003-2618-2458; RC, 0000-0001-6353-1464

*Correspondence: ardehez@aut.ac.ir

Abstract: Given the challenges in data acquisition and spatial modelling at the detailed exploration stage, it is difficult to develop a prospectivity model, particularly for disseminated ore deposits. Recently, the weights of evidence (WofE) method has demonstrated a high efficiency for modelling such deposits. In this study, we propose a framework for creating a three-dimensional (3D) WofE-based prospectivity model of the Nochoun porphyry Cu deposit in SE Iran. The input data include qualitative geological and quantitative geochemical information obtained from boreholes and field observations. We combine ordinary and fuzzy weights of evidence for integrating qualitative and quantitative exploration criteria in a 3D space constrained by a metallogenetic model of the study area for identifying a deep-seated ore body. Ordinary weights of evidence are determined for geological data, including lithology, alteration, rock type and structure. Moreover, we determine the fuzzy weight of evidence for each class of the continuous geochemical models created based on the factors analysis of Fe, Mo and Zn concentration values derived from boreholes. We integrate the input evidential models using WofE and create the posterior probability model. We also determine anomalous voxels in the probability model using a concentration–volume fractal model and validate them using a prediction–volume plot and test boreholes. The modelling results indicate the efficiency of the posterior probability model in identifying the anomalous voxels representing copper mineralized rock volumes. We provide open source software for the proposed framework which can be used for exploring deep-seated ore bodies in other regions.

Keywords: spatial modelling; three-dimensional prospectivity modelling; weights of evidence; uncertainty; porphyry Cu; nochoun

Supplementary data: Python scripts for implementing the proposed framework and [supplementary files](#) including more details on the evidential models are available at https://github.com/intelligent-exploration/3D_WofE.

Received 1 June 2020; revised 1 August 2020; accepted 4 August 2020

The increasing shortage of easily detectable, outcropping ore deposits has led more and more mineral explorers to prospect for concealed or deep-seated ore deposits, in particular for metals such as copper, which plays a crucial role in modern society (Mudd *et al.* 2013; Schodde 2013; Mudd and Jowitt 2018). With increasing depth, traditional exploration methods are progressively less efficient and/or more costly. Mineral prospectivity mapping has been developed and applied for various types of ore deposits and at a variety of scales ranging from continental to regional (Brown *et al.* 2000; Carranza *et al.* 2005; Carranza and Sadeghi 2010; Zuo *et al.* 2011; Rodriguez-Galiano *et al.* 2015; Chen and Wu 2017; Xiong and Zuo 2018; Shirmard *et al.* 2020). Whilst most prospectivity mapping methods can be categorized as either knowledge- or data-driven approaches (Cheng and Agterberg 1999; Porwal *et al.* 2003; Manap *et al.* 2013), hybrid methods consider both data and expert knowledge (Sun *et al.* 2019). The latter are typically used for identifying areas of high potential for the discovery of ore deposits in two-dimensional environments (Knox-Robinson 2000; Carranza *et al.* 2008; Porwal *et al.* 2010; Carranza and Laborte 2015).

Deep-seated ore deposits usually show weak exploration signals on the ground surface. Therefore, there is a need to develop two-dimensional (2D) mineral prospectivity mapping methods in three-dimensional (3D) space to benefit in-depth exploration of mineral resources. 3D modelling, analysis and visualization facilitate the perception of key spatial factors in mineralization, ore genesis, and

geologic evolution in addition to target appraisal (Carranza 2009; Payne *et al.* 2015; Zuo *et al.* 2016; Li *et al.* 2018; Mao *et al.* 2019). The ability of 3D modelling to provide a reliable spatial model is completely dependent on the quality of input datasets, modelling techniques, expert knowledge, and the complexity of the local geological setting (Houlding 1994; Fallara *et al.* 2006; Lindsay *et al.* 2012; Jessell *et al.* 2014; Liu *et al.* 2016). A comprehensive metallogenetic model such as those suggested for porphyry Cu deposits (Lowell and Guilbert 1970; Meng 1997; Berger *et al.* 2008; Sillitoe 2010), helps geometric modelling and spatial analysis through enhanced reliability of 3D models.

Several three-dimensional mineral prospectivity modelling methods have been developed in recent years (Yuan *et al.* 2014; Li *et al.* 2015; Nielsen *et al.* 2015, 2019; Xiao *et al.* 2015; Mao *et al.* 2019), which can be applied along with estimation methods, such as geostatistics, for modelling drilling data and detecting deep-seated ore deposits at both regional and local scales. Regional-scale 3D mineral prospectivity modelling and quantitative assessment is rarely feasible, because required public-domain datasets with consistent coverage over large areas are not available (Xiao *et al.* 2015). One of the advantages of 3D mineral prospectivity modelling over geostatistics is its ability to integrate different types of qualitative and quantitative exploration data rather than being restricted to modelling the concentrations of individual geochemical elements. Some information, such as geological

characteristics obtained from boreholes consume large amounts of time and money, which are surprisingly less considered at the stage of detailed exploration due to the lack of a specific framework for combining qualitative data with more favourable quantitative data. The 3D mineral prospectivity modelling methods are able to integrate such data and provide an efficient model for optimizing the process of selecting new drilling locations and planning the exploitation of an ore reserve.

In recent years, Bayesian modelling approaches have been applied to the modelling of geological features (Scalzo *et al.* 2019; Olieroor *et al.* 2020). The Bayesian inference approach is able to provide a fully quantitative and informative 3D prospectivity model and to fuse all available constraints in a probabilistically rigorous fashion. The weights of evidence (WoE) method is based on Bayes' rule (Xiao *et al.* 2015) and has been effectively used for 2D mineral prospectivity mapping of various types of ore deposits (e.g. Carranza 2004; Porwal *et al.* 2010; Pazand and Hezarkhani 2014; Kreuzer *et al.* 2015; Zeghouane *et al.* 2016). The fuzzy WoE method developed by Cheng and Agterberg (1999), prevents loss of information due to converting continuous models into binary models. This method has a number of advantages compared to other simpler or even more complicated data-driven methods. In general, the weights of evidence represent the degree of correlation between a target mineralization and a particular model or pattern created under specific conditions known as an evidence (Bonham-Carter *et al.* 1989; Agterberg *et al.* 1990; Cheng and Agterberg 1999; Carranza 2004; Yuan *et al.* 2014).

The response variable in 3D mineral prospectivity modelling is the concentration of target elements greater than a threshold value, while in 2D prospectivity mapping, the response variable is usually the presence/absence in a unit cell of a known mineral deposit. The number of deposits is usually quite small in contrast to the number of anomalous voxels in 3D modelling. Using 3D mineral prospectivity modelling, geological, geochemical and geophysical data can be integrated according to the known dispersion of mineralization in a modelling space. The result of this process is a formulated 3D model which presents a quantitative assessment of the probability of detecting a target mineralization based on exploration criteria. The exploration criteria must include all the factors which control a specific target mineralization in a study area (Yuan *et al.* 2014). They help to provide the 3D evidential models which are later used as inputs to the modelling process.

In this study, we extend and demonstrate the application of the WoE method in 3D space based on a proposed framework for modelling a porphyry copper (Cu) deposit located in SE Iran within a magmatic arc called Urmia-Dokhtar. We use borehole data consisting of qualitative geological and quantitative geochemical data along with surficial geological data for providing input for 3D evidential models. Based on the proposed framework, the ordinary and fuzzy WoE methods are used for weighting voxels in binary geological and continuous geochemical evidential models, respectively. We use the total variance associated with each voxel to assess uncertainty in the posterior probability model. The concentration–volume fractal models and prediction–volume plots are used to evaluate and validate our models. We provide Python scripts as open-source software for implementing the proposed framework in this study.

Geological setting

The Nochoun porphyry copper deposit is located within a magmatic arc subdivision called Urmia-Dokhtar where extensive Tertiary to Plio-Quaternary intrusive and extrusive units are exposed in a northwest-southeast trend (Fig. 1). In several studies, a subduction-related magmatic model is suggested for the Urmia-Dokhtar magmatic arc, which is known to be a result of the closure of the

Neo-Tethys ocean between Arabian and Eurasian plates (Berberian and Berberian 1981; Omrani *et al.* 2008). In general, this magmatic arc involves two major mineralization regions of Chahar Gonbad to the SE and Sungun to the NW. The dominant type of mineralization is porphyry Cu which is associated with Eocene, Pliocene and Quaternary plutonic bodies and volcanic rocks. The major lithological units of the study area, located in the Chahar Gonbad region in southeast Iran, consist of volcanic and subvolcanic complexes, and intrusive bodies. The volcanic rocks cover most of the study area and consist of Eocene andesite, dacite and rhyodacite associated with tuff breccias (Abedi *et al.* 2014). As shown in Figure 2, the intrusive bodies include granite to diorite dispersed in the S to SW of the study area.

Alteration and mineralization

The hydrothermal alteration and mineralization in the Nochoun porphyry copper deposit strike NE-SW and centre on a stock (Fig. 2). The early hydrothermal alteration was dominantly potassic and propylitic, followed later by phyllitic, silica, and argillic alteration types. The potassic alteration is represented by mineral assemblages developed pervasively as halos around veins in the central parts of the study area. There is a relatively sharp boundary between the propylitic and potassic alteration zones in deeper parts of the ore deposit, but this contact is obscured by later phyllitic alteration in shallow levels. The propylitic alteration is pervasive and represented mainly by chloritization of primary and secondary biotite and groundmass materials of the rocks which are peripheral to the central potassic zone (Fig. 2). The plagioclase minerals were replaced with epidote, but this alteration is less pervasive and less intense compared to the chloritization. Feldspar minerals are locally altered to clay minerals in shallow levels and the dominant mineral is kaolinite accompanied by illite. Moreover, the entire rocks have been altered to an assemblage of clay minerals, hematite and quartz close to the erosion surface which are soft and white. The shallow alteration is interpreted to represent a supergene blanket over the ore deposit and the alteration of feldspar to clay in depth may have the same origin. Also, the latter may represent an argillic stage of the hypogene alteration.

The hypogene copper mineralization was disseminated or emplaced in veinlets during phyllitic alteration and to a lesser extent potassic alteration. During the potassic alteration, the copper was deposited as chalcopyrite and minor bornite; later hypogene copper was deposited mainly as chalcopyrite. The rocks are highly altered at the exposed surface of the ore deposit and the only mineral which has survived alteration is quartz. Most of the sulfide minerals have been leached, and copper has been concentrated in an underlying supergene zone by downward percolating groundwater. In general, the mineralization in the study area is the result of two geological processes including the intrusion of a granodiorite body and the ascension of hydrothermal fluids. The mineralization-bearing rocks hosted by the granodiorite body usually appear in veins with a thickness of 2–3 m, and they are mostly found in the marginal sections of the host body or tuffaceous units. This type of mineralization is considered non-economic due to the low grade. Different types of ore minerals such as hematite, magnetite and malachite with intense silicification of the veins are observed in mineralization zones (Fig. 3). Moreover, polished sections of mineralized rocks, show the presence of chalcopyrite, pyrite and sphalerite (Fig. 4). There are a number of stockworks exposed on the surface which are the result of hydrothermal fluid interaction (Fig. 2). These stockworks are probably related to the intrusion of dykes and quartz monzonite apophyses. In this type of mineralization, malachite and azurite are found on the surface along with minor chalcopyrite as inclusions within quartz (Abedi *et al.* 2014).

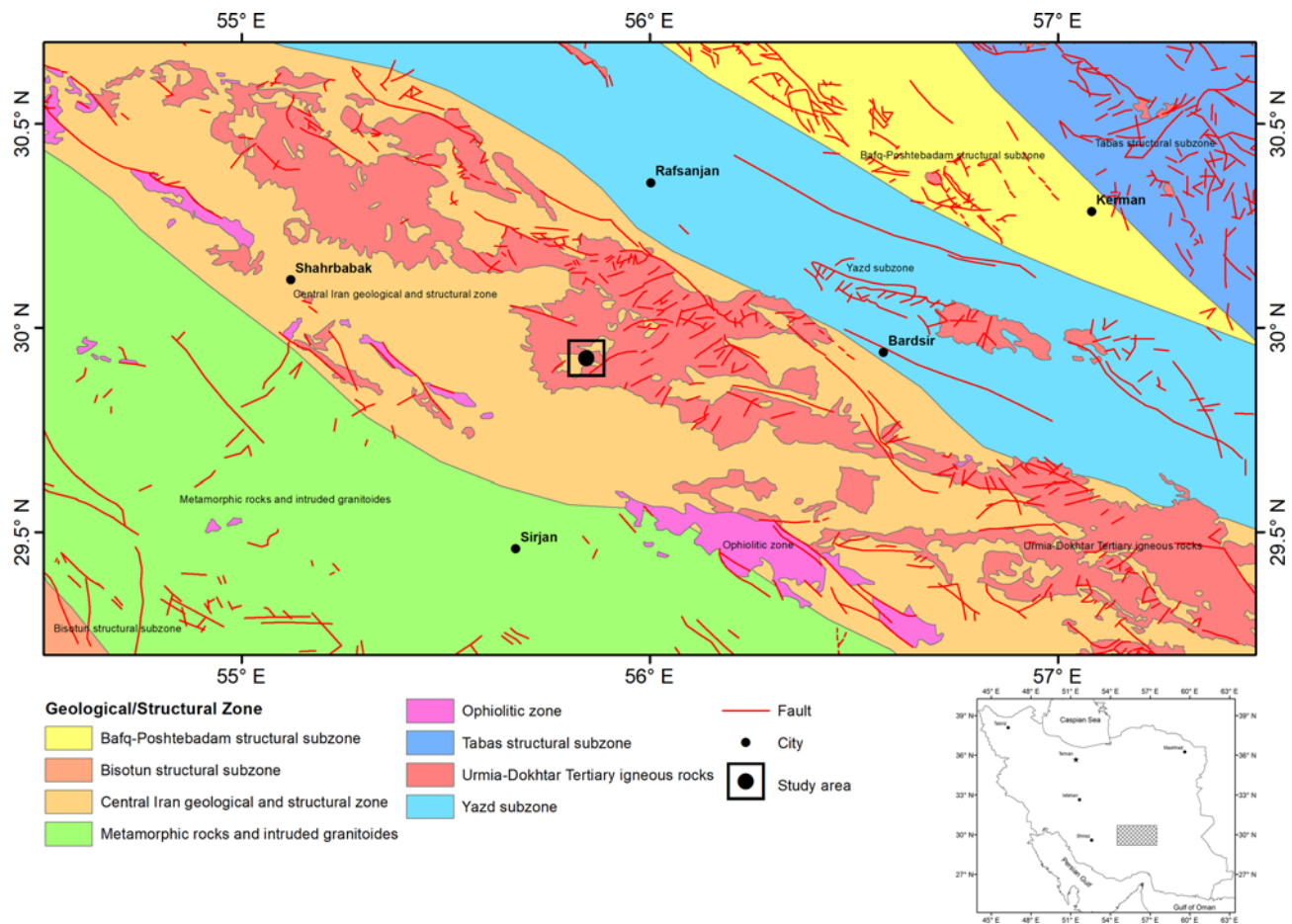


Fig. 1. A portion of the Chahar Gonbad region located in southeast Iran within the Urmia-Dokhtar magmatic arc. The study area is shown at the centre of the map in a black square.

Materials and methods

Drilling data

There are 113 boreholes in the study area which provide detailed qualitative geological and quantitative geochemical data. The data obtained from seven boreholes scattered in the study area are considered as test data and the rest are employed for training and creating 3D evidential models (Fig. 5). The size of each voxel in the 3D models according to the extent of the modelling space is determined to be $10 \times 10 \times 10$ meters (m). The geometrical parameters of the modelling space can be found in Table 1. We inscribe the 3D models in a polygon created by the convex hull algorithm based on the coordinates of the borehole collars on the ground surface (Fig. 5). Moreover, they are restricted to a super- and sub-face based on the elevation of the borehole collars and the depth of each borehole to make sure there are a sufficient number of data points for interpolation throughout the modelling space. The total number of voxels is *c.* 500 000.

The geological data used for creating 3D geological evidential models involve lithology, alteration and rock type information. In addition to Cu concentration values used for creating the training model, we use other geochemical data including the concentration values of key elements for providing 3D geochemical evidential models. The 3D strip-logs of the geological data and Cu concentration are shown in Figures 6 and 7, respectively.

Structural data

The drilling data used in this study do not involve structural data such as the position of faults in depth. Therefore, we extend surficial

structural data to depth to create 3D fault surfaces. The available surficial data include some information about the strike, dip and dip direction of the faults which have been provided by fieldwork, and validated by remote sensing data (Farahbakhsh *et al.* 2019a). The faults include those exposed on the surface or those, known as concealed faults, covered by a thin layer of regolith. A 3D model of the fault surfaces called 3D ribbons is created using the available data and then restricted to the modelling space. This model is later converted into a 3D block model to be used as a structural evidential model.

3D modelling

Geological modelling

As shown in Figure 5, there are a high number of boreholes in a small area which makes it possible to create a precise 3D geological model using the drilling data. In this study, we use a basic interpolation method called closest point for interpolating qualitative geological data including lithology, alteration, and rock type in a 3D space with the RockWorks software package (RockWorks17 2019a). The value of a voxel node is set to be equal to the value of the nearest data point, regardless of its distance from the point or the value of its other neighbours. One of the advantages of this method is that the solid model nodes will honour the control points. This method can be used for modelling complex non-stratiform geology (e.g. multiple intrusions, impact craters, karst, etc.) such as our study area. The 3D geological evidential models are constrained to the geological map presented in Figure 5. Moreover, the lithological model is constrained to the cross-sections shown in Figure 8 drawn based on the drilling data and geological knowledge.

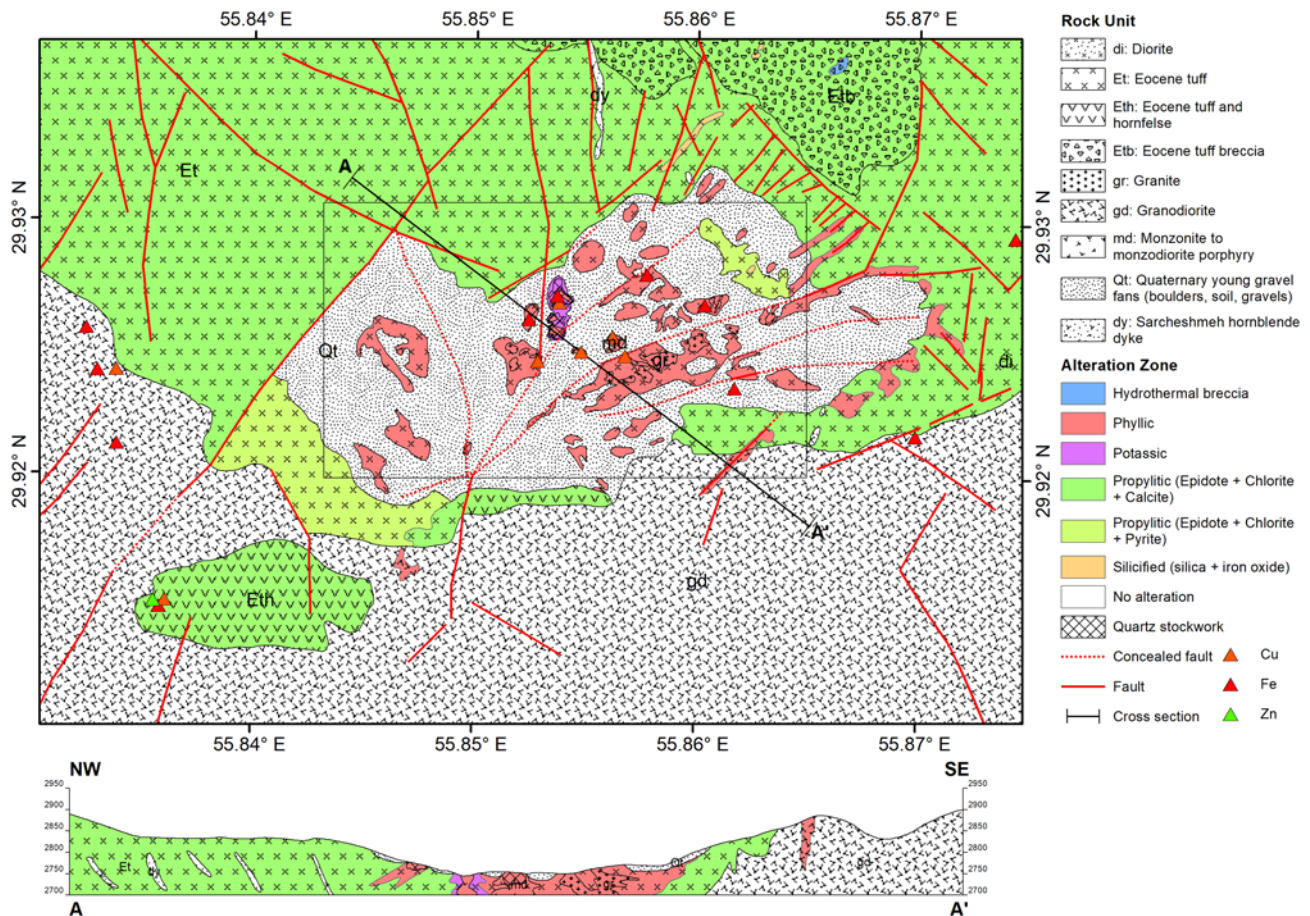


Fig. 2. Detailed geological and alteration map of the study area along with a cross-section intersecting some of the mineral occurrences. The black rectangle shows the study area.

Geochemical modelling

The concentration values of different elements have been assayed along the boreholes. However, the number of samples are different. We investigated the bivariate correlation between different elements and Cu concentration values. According to the results, iron, molybdenum and zinc (Fe, Mo and Zn) show a high correlation and they involve the highest number of samples. These elements are usually applied through prospecting for porphyry Cu deposits (Xiao *et al.* 2014; Farahbakhsh *et al.* 2019b). Moreover, these elements are known as the key indicators of porphyry Cu mineralization in the study area. It is assumed that conditional independence exists when combining two or more evidential models with the Bayesian inference (Bonham-Carter 1994). In practice, conditional independence is often violated to some degree and to avoid it as much as possible, we combined geochemical data into two factors using factor analysis available with the IBM SPSS Statistics software

package (IBM Corp. 2019). The output factors are statistically uncorrelated with one another, so that the likelihood of violating conditional independence is greatly reduced (Farahbakhsh *et al.* 2019b). Geochemical data are known as compositional data which suffer from the closure problem and need to be transformed using a log ratio transformation before factor analysis (Filzmoser *et al.* 2009; Carranza 2011). In this study, we use isometric log-ratio (ilr) transformation available with the CoDaPack software package (Comas-Cufí and Thió-Henestrosa 2011) to transform raw data which has some theoretical advantages over other log-ratio transformations for statistical analysis of geochemical data (Filzmoser *et al.* 2009).

We use the inverse-distance anisotropic modelling method which is one of the different kinds of inverse-distance algorithms for interpolating the factors in a 3D space. This method has been widely used for interpolating continuous variables both in two- and three-

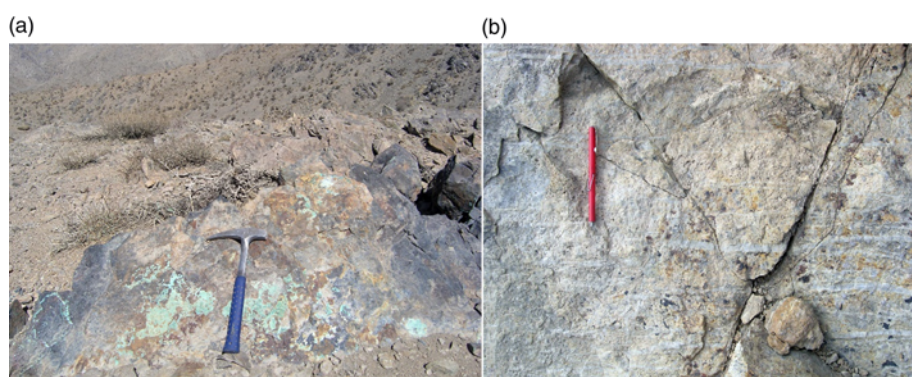


Fig. 3. (a) Cu oxide minerals including malachite and azurite in fractures of silicified tuff crystals; (b) quartz veinlets with a stockwork texture.

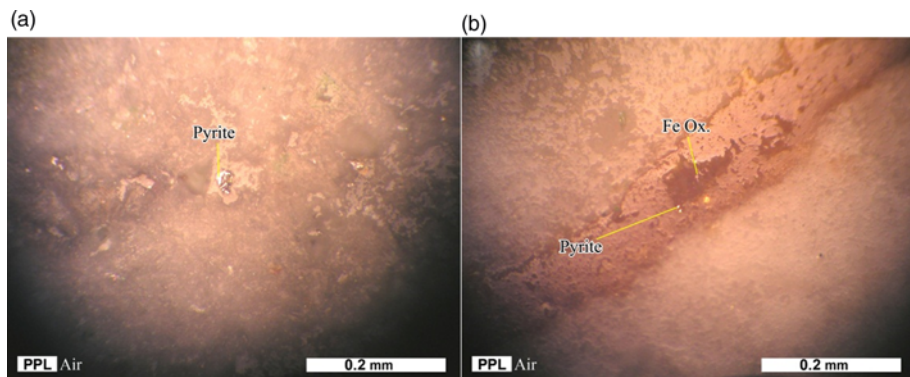


Fig. 4. Polished sections showing the presence of (a) pyrite, and (b) iron oxide crystals in mineralized rocks.

dimensional models (e.g. Zuo 2011; Wang and Huang 2012). Using the inverse-distance in general, we assign a voxel node value based on the weighted average of neighbouring data points, and the value of each data point is weighted according to the inverse of its distance from the voxel node, taken to a power. The greater the value of the exponent, the less influence distant control points will have on the assignment of the voxel node value (Zuo *et al.* 2016; RockWorks17 2019b). Using the inverse-distance anisotropic method, we look for the closest control point in each 90-degree sector around the node. In this study, the weighting exponent is set to 2, experimentally. The directional search can improve the interpolation of voxel values that lie between data point clusters, and can be useful for modelling borehole-based data. The quadrant searching tends to connect the limits (highs and lows) at the same elevation.

Weights of evidence modelling

The WoFS method is a well-known and robust data-driven prospectivity modelling method based on the Bayesian theorem (Bonham-Carter 1994). This method is used for estimating the posterior probability of detecting an ore body under the assumption

of conditional independence of input evidential models (Xiao *et al.* 2015). This assumption is also known as one of the weaknesses of this method (Joly *et al.* 2012). The WofE method can work with a lower number of training datasets compared to other data-driven or machine learning techniques. Using this method, the prior probability of detecting a specific type of mineralization in an area or space is updated in the light of other evidence such as geological, geochemical or geophysical models. An example of the prior probability is the primary or training model created by interpolating the concentration values of the target element obtained through boreholes. In this study, we interpolate Cu concentration values as well as other geochemical elements, and then the interpolated model is converted into a binary model to determine the approximate target ore body. In general, the posterior probability of mineralization ($P(M)$) after looking at evidence (E) is determined via the likelihood function using equation (1) (Bonham-Carter 1994).

$$P(M|E) = P(M) \frac{P(E|M)}{P(E)} \quad (1)$$

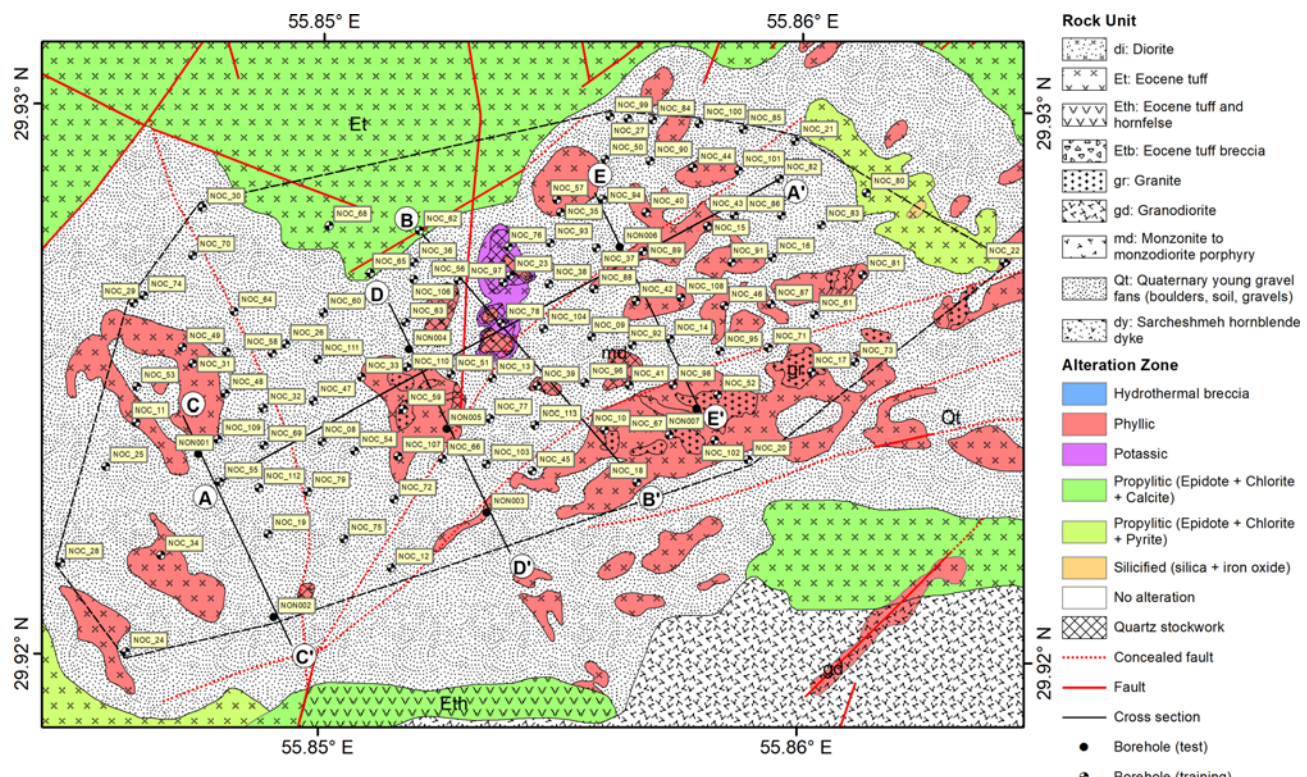


Fig. 5. Borehole collars along with their identification labels shown on the geological map of the study area enlarged from Figure 2. The polygon drawn around the borehole collars shows the boundaries of the modelling space.

Table 1. Geometrical parameters of the 3D modelling space

Parameter	Value
North-South extent	970 m
East-West extent	1740 m
Vertical extent	890 m
Polygon area on the surface	0.8841 km ²

This method is simple from the computational view, and the 2D WoFE method is readily implemented using GIS packages (e.g. ArcGIS Desktop 2019; QGIS Development Team 2019); however, implementing this method in 3D space is more complicated. In this study, we deal with binary or discrete geological and continuous geochemical evidential models. Therefore, to minimize the loss of information, we determine ordinary positive and negative weights for each unit of the geological models and a fuzzy weight for each class of the geochemical models. In binary models, the weights of

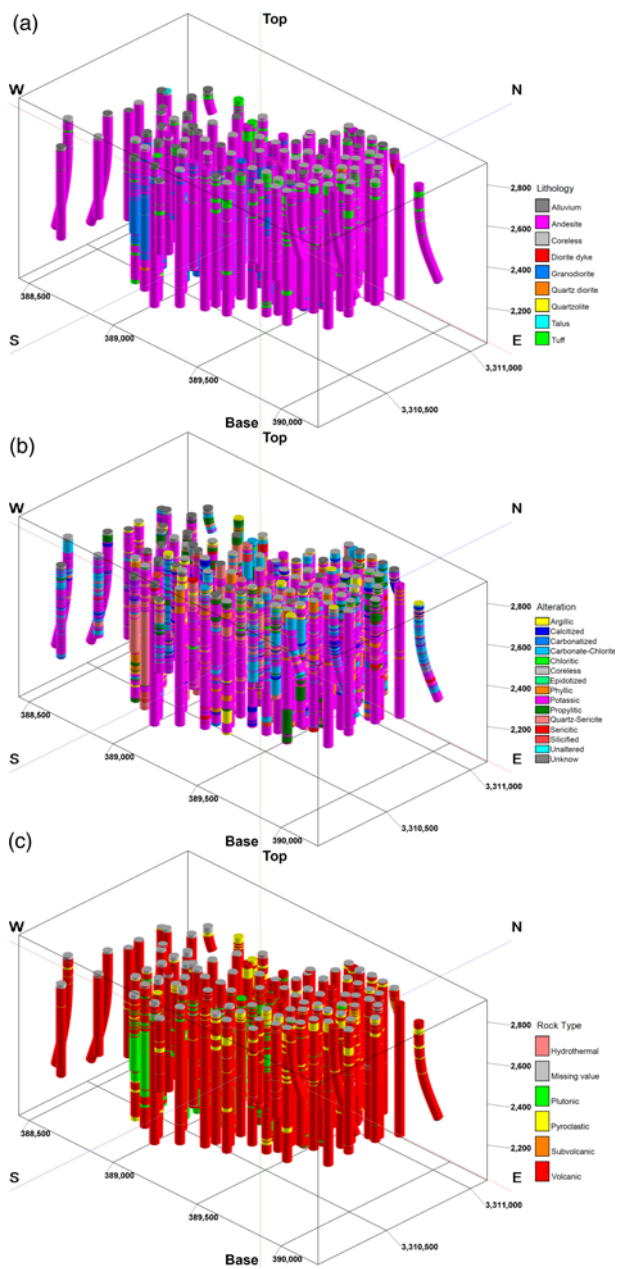


Fig. 6. 3D strip-logs of the geological data including (a) lithology, (b) alteration, and (c) rock type.

evidence enable a user to interpret positive and negative weights in geological terms intuitively. The positive (W^+) and negative (W^-) weights are determined using equations (2) and (3) (Bonham-Carter 1994).

$$W^+ = \ln \frac{P(E|M)}{P(\bar{E}|M)} \quad (2)$$

$$W^- = \ln \frac{P(\bar{E}|M)}{P(\bar{E}|\bar{M})} \quad (3)$$

These weights indicate the spatial association between the voxels with and without mineralization, and the presence and absence of anomalous voxels in evidential models, respectively. For example, an evidential or predictor model can be used to assess the contribution of a geological process in the formation and prospectivity of a specific type of mineralization (Xiao *et al.* 2015). Investigating the contrast (C) which is determined using equation (4), can help with this assessment (Bonham-Carter 1994).

$$C = W^+ - W^- \quad (4)$$

High values of contrast show strong association of an evidential model with the mineralization process. The contrast is used to calculate the fuzzy weight of each class in continuous models. In this study, we classify geochemical evidential models based on the percentile to remove the effect of number of voxels on the fuzzy weight. Each model has ten classes with an equal number of voxels and a fuzzy membership function is created for each set of contrasts for different continuous evidential models. The contrast values are transformed to the fuzzy space ranging from 0 to 1 using the linear function (Bonham-Carter 1994) and called fuzzy contrast ($\mu_E(C)$). The fuzzy weight ($W\mu_E(C)$) for each class of continuous models is determined using equation (5) (Cheng and Agterberg 1999).

$$W_{\mu_E(C)} = \ln \frac{\mu_E(C)P(E|M) + (1 - \mu_E(C))P(\bar{E}|M)}{\mu_E(C)P(E|\bar{M}) + (1 - \mu_E(C))P(\bar{E}|\bar{M})} \quad (5)$$

The posterior probability model is the result of integrating input evidential models, which is generated using Bayes' equation in a log-linear form (equation 6) with the assumption that conditional independence applies (Bonham-Carter *et al.* 1989; Bonham-Carter 1994).

$$P_{\text{Pst}} = \frac{O_{\text{Pst}}}{1 + O_{\text{Pst}}} \quad (6)$$

where, P_{Pst} denotes the posterior probability and O_{Pst} is the posterior odds. The posterior odds equal the exponent of the posterior logit which can be determined by equation (7) (Bonham-Carter 1994; Cheng and Agterberg 1999).

$$\ln O(M|E_1 E_2 \dots E_k) = \ln O(M) + \sum_{i=1}^m W_i^{+-} + \sum_{j=1}^n W_{\mu_j} \quad (7)$$

where, there are k evidential models including m discrete and n continuous models. We use the aggregate of positive or negative weights in discrete models and the fuzzy weights in continuous models, with the prior logit of mineralization in the study area for calculating the posterior logit.

Using the WoFE method enables the user to calculate the effects of uncertainty on the weights, and uncertainty due to missing information. This leads to producing an uncertainty-quantified model which is propagated in the decision making. The variances of the weights and contrast help to model the uncertainty of the posterior probability due to uncertainty in the weights and caused by lack of information. The variance of positive ($\delta^2 W^+$) and negative ($\delta^2 W^-$) weights in discrete models are determined as presented in

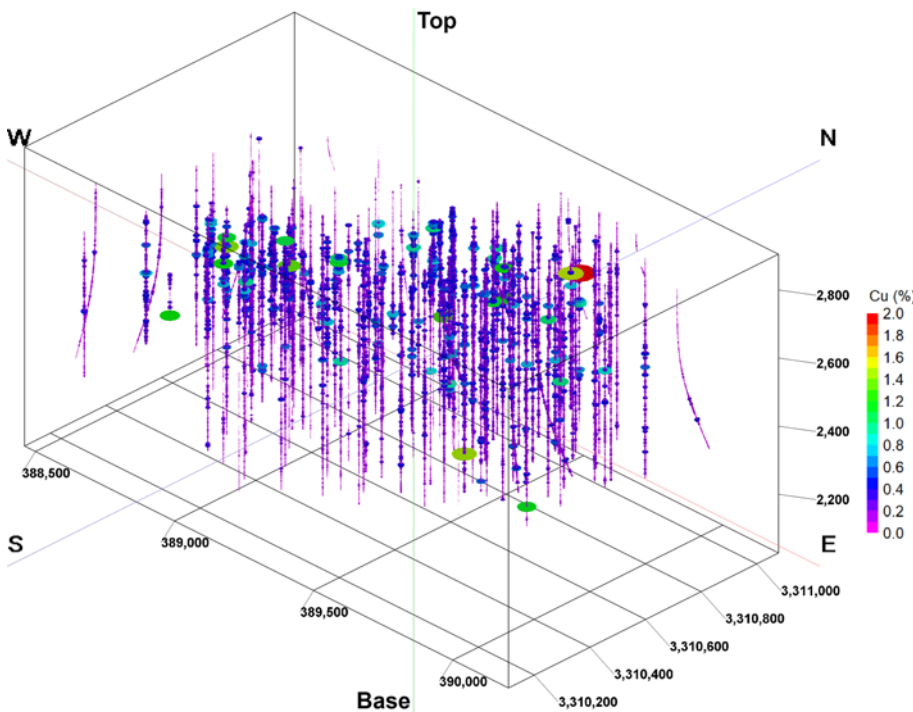


Fig. 7. 3D strip-logs of Cu concentration; the size and colour of cylinders shown along the boreholes are proportionate to the intensity of concentration.

equations (8) and (9), respectively (Bonham-Carter 1994).

$$\sigma_{W^+}^2 = \frac{1}{N(E \cap M)} + \frac{1}{N(E \cap \bar{M})} \quad (8)$$

$$\sigma_{W^-}^2 = \frac{1}{N(\bar{E} \cap M)} + \frac{1}{N(\bar{E} \cap \bar{M})} \quad (9)$$

where, N is the number of voxels and the variance resulting from the membership function μ_E can be expressed as equation (10). It has to be noted that we have assumed $P(E) + P(\bar{E}) = 1$.

$$\sigma_{\mu_E}^2 [P(M)] = \frac{2\mu_E(1 - \mu_E)}{P(\mu_E)} \sigma^2[P(M)] \quad (10)$$

where, $P(\mu_E)$ denotes the probability of the membership function and is determined using equation (11). Also, $\sigma^2[P(M)]$ is the variance of the prior probability of mineralization as given by

equation (12).

$$P(\mu_E) = \mu_E P(E) + (1 - \mu_E) P(\bar{E}) \quad (11)$$

$$\begin{aligned} \sigma^2[P(M)] &= \{P(M|E) - P(M)\}^2 P(E) \\ &+ \{P(M|\bar{E}) - P(M)\}^2 P(\bar{E}) \end{aligned} \quad (12)$$

A useful measure is to calculate the studentized value of contrast (C_{St}), as a measure of the uncertainty with which the contrast is known. We calculate the studentized value as the ratio of contrast to its standard deviation $S(C)$ as shown in equation (13).

$$C_{St} = \frac{C}{S(C)} \quad (13)$$

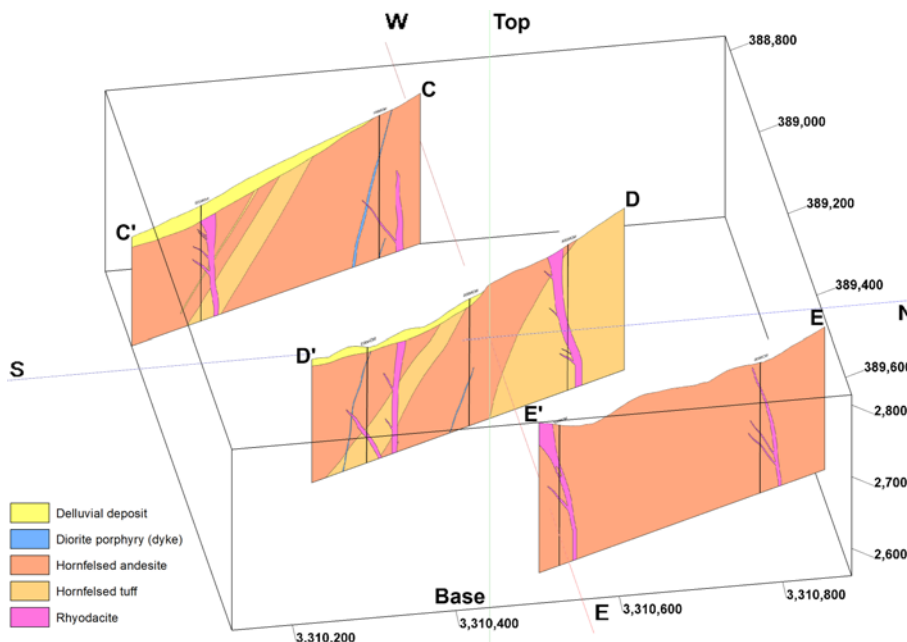


Fig. 8. Lithological cross-sections presented in a 3D view. The 3D lithological evidential model is constrained to these sections, in addition to the geological map.

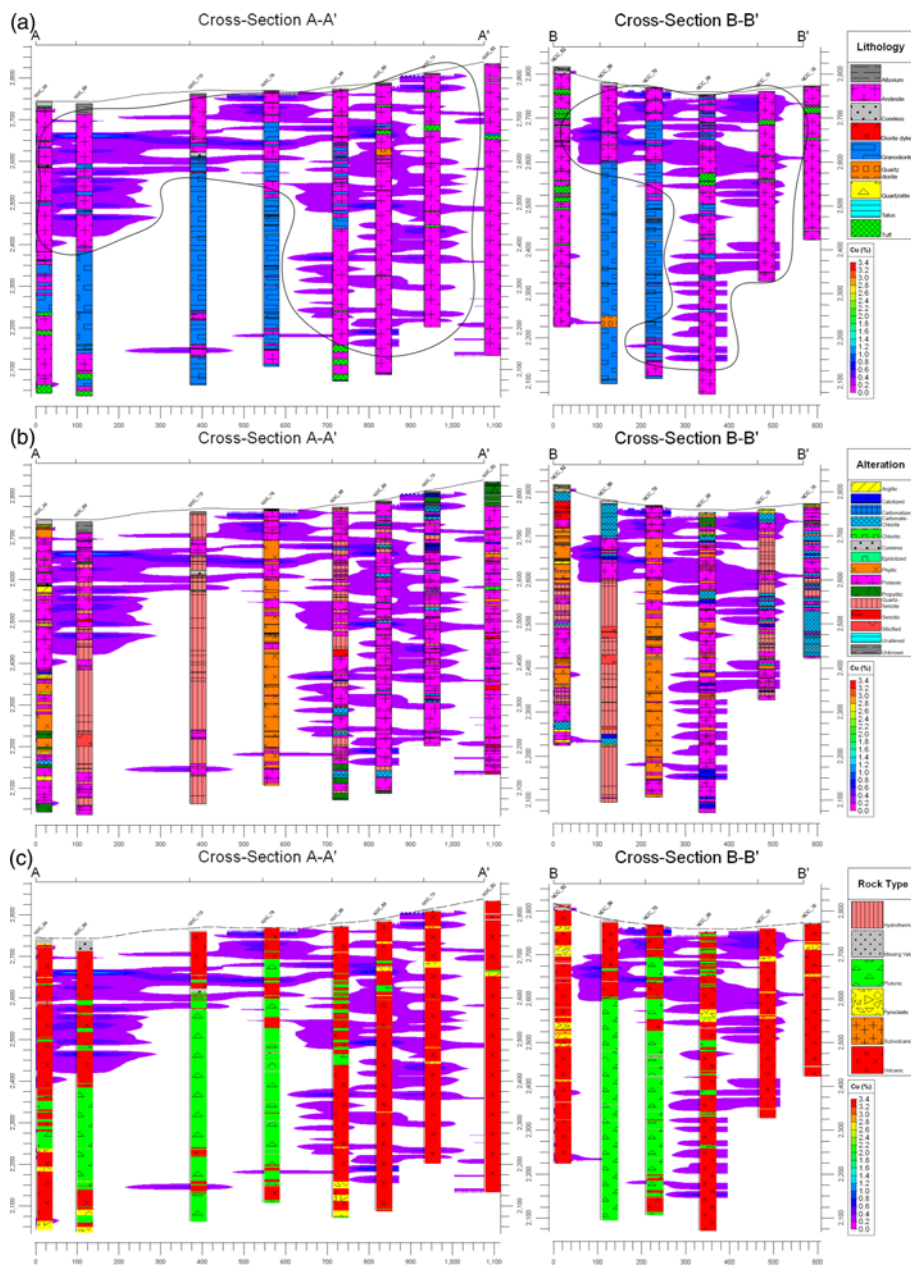


Fig. 9. Cross-sections AA' and BB' (Fig. 5) illustrated using (a) lithology, (b) alteration, and (c) rock type data obtained from the boreholes. The Cu concentration anomaly zones are shown in the background and outlined using the black lines.

The standard deviation of contrast is determined using equation (14).

$$S(C) = \sqrt{\sigma_{W^+}^2 + \sigma_{W^-}^2} \quad (14)$$

A large studentized contrast implies that the contrast is large compared with the standard deviation, and that the contrast is more likely to be real. A studentized value larger than 2, or even 1.5 is satisfactory (Bonham-Carter 1994). Due to the assumptions required for a formal statistical test, particularly the problem with the dependence of the standard deviation of contrast on the units of measurement, it is best to use this ratio in a relative, rather than an absolute sense (Bonham-Carter 1994). We use the variances of the weights to calculate the variance of the posterior probability at each voxel, and to generate an uncertainty model. The voxels where the variance is above some threshold can be masked out, due to lack of confidence in the result. In this study, the threshold is determined based on the concentration-volume (C-V) fractal model (Afzal *et al.* 2011).

In mineral prospectivity modelling, where the prior probability is assumed to be the average known mineralization point density, a simple test can be applied to determine the total number of predicted

mineralization voxels. If the total predicted number of voxels is much larger than the total observed number, it suggests that conditional independence is being violated. The predicted number (N_p) is determined using equation (15) by adding together the product of the area in unit cells (A) and the posterior probability (P) for all the voxels (Bonham-Carter 1994).

$$N_p = \sum_{i=1}^n P_i A_i \quad (15)$$

where there are n voxels in the model. In practice, the predicted number is always larger than the observed number with the weights of evidence. If the predicted number is more than 10–15% larger than the observed number, then a serious check of the pairwise tests and remedial action is in order (Bonham-Carter 1994). As described above, the three-dimensional WoFE method used in this study is similar to the traditional method applied for mineral prospectivity mapping (Bonham-Carter 1994; Cheng and Agterberg 1999; Carranza 2004), and pixels are replaced with voxels. We propose a framework for implementing the method in 3D space and

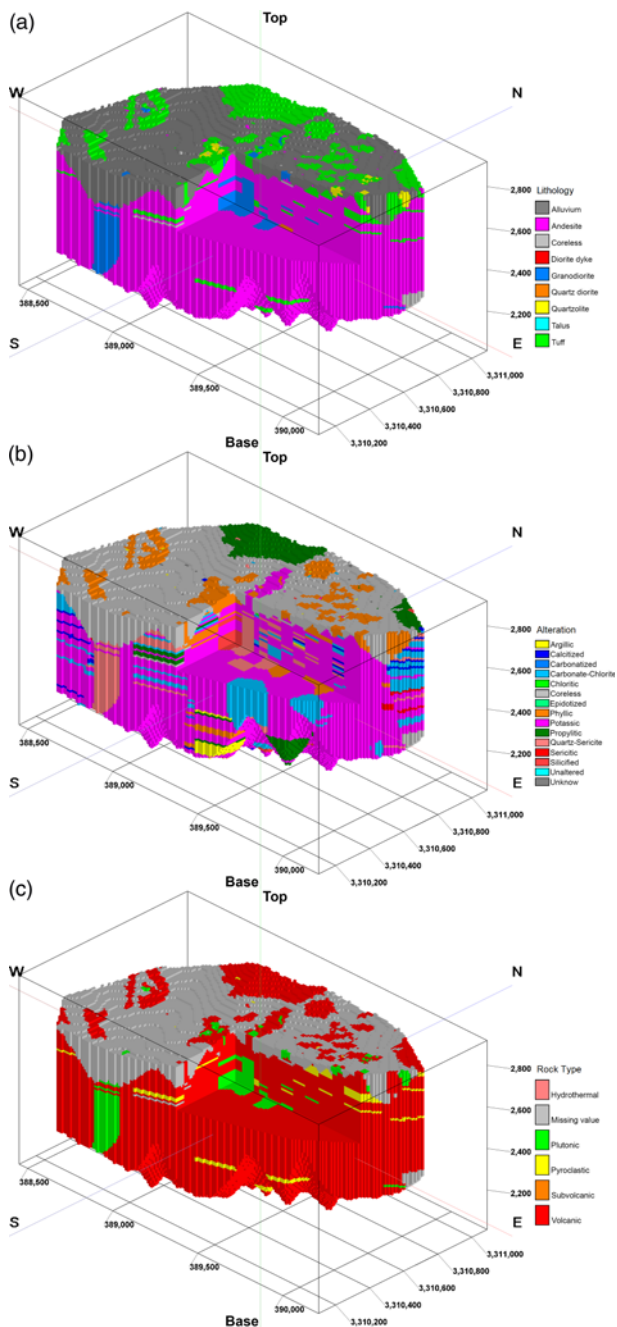


Fig. 10. Solid models created using (a) lithology, (b) alteration, and (c) rock type data. Each solid model is shown with a cutout.

summarize the steps to be taken for 3D mineral potential modelling using the WoE method in the following:

- acquiring data including required geological and geochemical data;
- dividing data into training and test categories;
- creating a primary model of the target mineralization based on the Cu concentration values obtained along the boreholes in different intervals;
- providing 3D geological and geochemical evidential models;
- calculating the weights of evidence and other necessary parameters such as the standard deviation and variance of the weights for different geological units and each class of geochemical models;
- selecting input evidential models for creating the posterior probability model based on the contrast and studentized contrast;

- integrating selected evidential models and creating 3D posterior probability model;
- removing the voxels associated with high uncertainty;
- investigating the conditional independence and validating the results.

Results

3D evidential models

We use three different types of geological data including lithology, alteration, and rock type for creating 3D geological evidential models. As shown in Figure 5, we designed two cross-sections (AA' and BB') along the small and large diameters of the study area to visually investigate the correlation between the aforementioned data types and Cu concentration. These cross-sections along with the interpolated Cu concentration anomaly zones (greater than 0.2%) are shown in Figure 9. The geological evidential models created using the closest point method are constrained to the geological map and three cross sections (Figs 5 and 8) to be more reliable. The output solid models are presented in Figure 10.

The 3D ribbon model of the faults is converted into a block model. The size of each voxel in this model is the same as other evidential models. Moreover, we use two buffer zones with a radius of 25 and 50 m surrounding the fault blocks to investigate the correlation of proximity to the faults and Cu mineralization. An overall model of the fault blocks and different buffer zones is presented in Figure 11.

We use Cu concentration values in different intervals through the boreholes to create a primary 3D model of the target ore body concealed in depth using the inverse-distance anisotropic interpolation method which is later used as a training model. Moreover, we use the factors obtained from factor analysis on geochemical elements for creating geochemical evidential models. According to the cutoff grade of Cu in the ore deposits located in the neighbourhood of our study area such as Sarcheshmeh (Waterman and Hamilton 1975), the threshold for creating a binary model of the target ore body is considered 0.4%. Based on this threshold, the target ore body occupies less than 3% of the total modelling space, which can also be considered as the prior probability (Fig. 12). Here the number of anomalous voxels is large which is a rather different modelling situation from the 2D mineral prospectivity mapping.

Prospectivity modelling

Based on the equations presented in the Weights of evidence modelling section, the ordinary weights of evidence for geological evidential models are determined (Table 2). We consider every unit of lithology, alteration and rock type data as a binary model in order to determine the weights of evidence, contrast and studentized contrast. Those lithology and alteration, and rock types as well as structural models which are not found in this table show negative contrast and they were removed from the modelling process. One of the reasons for this can be the low number of occupied voxels, and hence low number of common voxels with the target ore body. More details can be found in the supplementary file. The fuzzy weight along with other parameters is determined for each class of the geochemical factors. In Tables 3 and 4, we present the results for the first and second factors, respectively. It is noteworthy that we use all of the classes, even those with negative contrast, in the modelling process.

All the evidential models presented in Tables 2–4, are integrated as described in the Weights of evidence modelling section and a posterior probability model is the result. We removed a small number of voxels due to high total variance which occupies less than 1% of the modelling space and used the C-V fractal model for classification and determining a proper threshold for separating anomalous voxels.

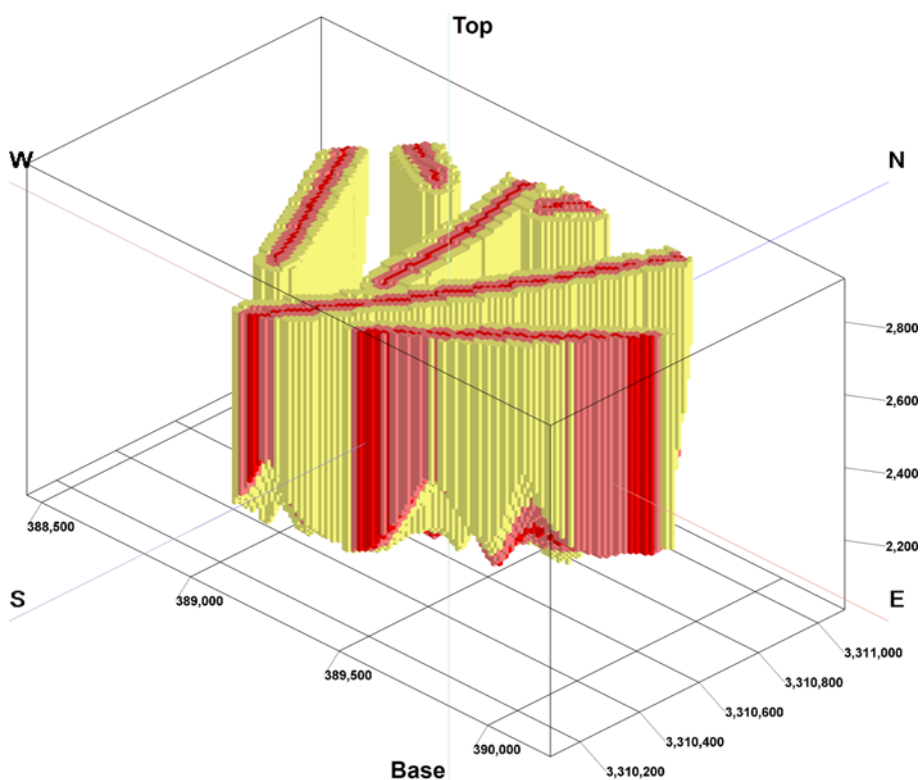


Fig. 11. Block model of the fault surfaces surrounded by two buffer zones in a radius of 25 and 50 m.

According to the C-V chart presented in Figure 13a, the voxels showing a posterior probability greater than 0.17 are considered as the certain anomaly. Also, the voxels showing a value greater than 0.14 and 0.04 can be considered as the probable and possible anomaly, respectively. In Figure 13b, the classified posterior probability model and the voxels with values greater than 0.17 are shown which occupy nearly 1% of the modelling space. The predicted number of mineralization voxels in the posterior model is nearly 12% larger than the observed number, then there is no need to check the pairwise tests and we can assume the conditional independence between input evidential models applies.

Validation

In 2D mineral prospectivity mapping, a prediction-area plot is used in order to quantitatively validate the results obtained from prospectivity maps (Yousefi and Carranza 2015). We extend the application of these types of plots to three-dimensional space and call them prediction-volume (P-V) plots. In P-V plots, we show the cumulative percentage of predicted mineralization and the corresponding cumulative occupied volume, with respect to the total volume against the prospectivity values. Therefore, the prediction ability of a prospectivity model and its ability to delimit the

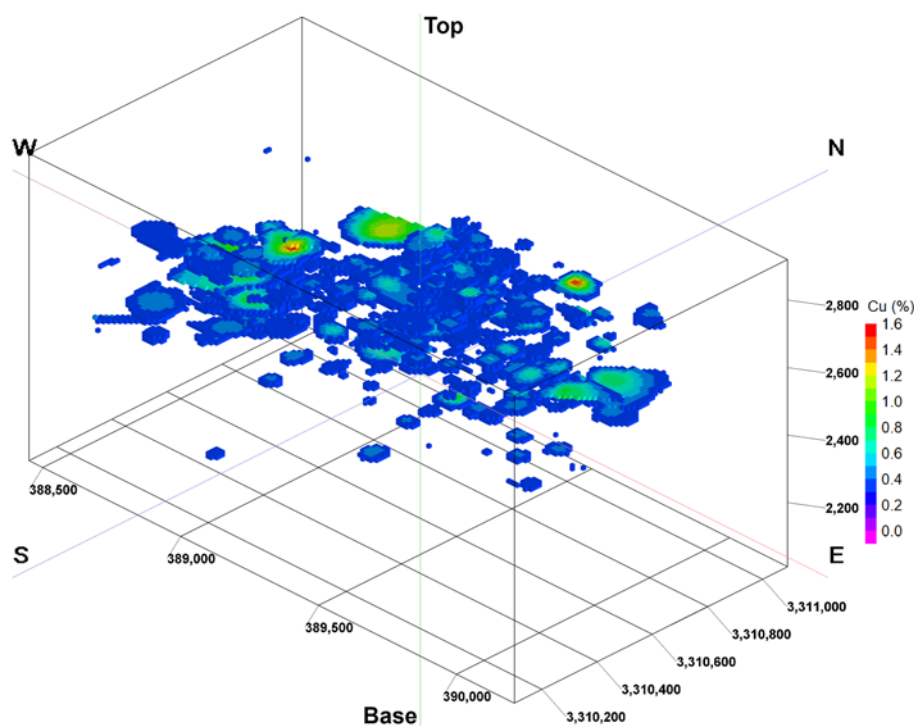


Fig. 12. Anomalous voxels of the 3D geochemical model created using the concentration value of Cu.

Table 2. Variation of the ordinary weights of evidence, contrast and studentized contrast with different lithology, alteration, and rock types

	W^+	W^-	Contrast	Studentized contrast
Lithology				
Andesite	0.0186	-0.0776	0.0962	4.4241
Granodiorite	0.2635	-0.0276	0.2911	10.6316
Diorite dyke	0.5362	-0.0003	0.5365	1.6569
Alteration				
Carbonatized	0.4878	-0.0027	0.4905	4.7330
Epidotized	2.4821	-0.0001	2.4822	3.0399
Silicific	0.9991	-0.0140	1.0131	17.0737
Potassic	0.1497	-0.2302	0.3799	21.4171
Rock type				
Volcanic	0.0244	-0.1220	0.1464	6.2926

Table 3. Variation of the fuzzy weights of evidence and other important parameters with different classes of the first geochemical factor

Lower limit	Upper limit	W^+	W^-	Contrast	Studentized contrast	Fuzzy contrast	Fuzzy weight
Min	-1.2255	-2.1868	0.0965	-2.2833	-29.1108	0.2160	0.0688
-1.2255	-0.6158	-1.5931	0.0868	-1.6799	-28.6091	0.3250	0.0436
-0.6158	-0.2882	-1.2428	0.0777	-1.3205	-26.6084	0.3899	0.0268
-0.2882	-0.0804	-1.4786	0.0842	-1.5628	-28.1291	0.3462	0.0382
-0.0804	0.0821	-1.0541	0.0713	-1.1254	-24.8064	0.4251	0.0176
0.0821	0.2285	-0.8674	0.0635	-0.9309	-22.3942	0.4602	0.0088
0.2285	0.3729	-0.4526	0.0401	-0.4927	-14.3323	0.5394	-0.0062
0.3729	0.5330	0.1976	-0.0244	0.2220	8.5314	0.6684	0.0198
0.5330	0.7502	0.7893	-0.1381	0.9274	44.3317	0.7958	0.2338
0.7502	Max	1.5767	-0.4817	2.0584	117.5165	1.0000	1.5767

Table 4. Variation of the fuzzy weights of evidence and other important parameters with different classes of the second geochemical factor

Lower limit	Upper limit	W^+	W^-	Contrast	Studentized contrast	Fuzzy contrast	Fuzzy weight
Min	-0.7221	-1.0799	0.0722	-1.1521	-25.0827	0.4194	0.0190
-0.7221	-0.4092	-0.5885	0.0489	-0.6373	-17.4375	0.5122	-0.0022
-0.4092	-0.2144	-0.1276	0.0133	-0.1409	-4.7295	0.6016	-0.0059
-0.2144	-0.0675	0.1477	-0.0177	0.1654	6.2313	0.6568	0.0132
-0.0675	0.0632	0.2323	-0.0293	0.2615	10.1954	0.6741	0.0248
0.0632	0.1941	0.2040	-0.0253	0.2293	8.8381	0.6683	0.0205
0.1941	0.3400	0.1792	-0.0219	0.2012	7.6749	0.6633	0.0171
0.3400	0.5142	0.2985	-0.0390	0.3375	13.5068	0.6878	0.0364
0.5142	0.7965	0.1280	-0.0152	0.1432	5.3524	0.6528	0.0110
0.7965	Max	-0.0789	0.0084	-0.0873	-2.9907	0.6113	-0.0041

modelling space for further exploration and drilling are evaluated in a scheme. The P-V plot shows a curve of the percentage (prediction rate) of known mineralization and a curve of the percentage of occupied volume corresponding to the classes of a prospectivity model. When an intersection point of the two curves is at a higher place, it portrays a small volume containing a large number of mineralization-bearing voxels. The P-V plot of the posterior probability model is presented in Figure 14, indicating that more than 60% of the known anomalous voxels have been predicted in less than 40% of the modelling space. It is noteworthy that for assigning probabilistic values to the model in terms of prospecting for Cu mineralization, and distribution of the voxel values between 0 and 1, we transformed the data to fuzzy space using the linear function.

In addition to the P-V plot, we compare the posterior probability and Cu concentration values along the test boreholes and determine Pearson correlation coefficient (Pearson 1895) for each. It is observed that NON001, NON004, NON005 and NON006 show a coefficient above 0.5, NON007 is near 0.5 and the coefficient for NON002 and NON003 is under 0.5. In Figure 15, the graphs show

the variations of the posterior probability and Cu concentration along three of the test boreholes with a correlation coefficient above 0.5.

Discussion

Most of the study area is covered by alluvium, therefore the surface outcrop does not allow the lithology and alteration assemblages to be identified as detailed as the drill cores. In this study, we used two different types of drilling data including qualitative geological and quantitative geochemical data obtained from the boreholes through creating a 3D prospectivity model of Cu mineralization. The geological data comprise three types of data including lithology, alteration and rock type. Among the lithology types, andesite, granodiorite and diorite dyke show positive contrast and studentized contrast (Table 2) which were used as input binary models to the modelling process. The diorite dykes which involve a small portion of the modelling space show the highest contrast and a relatively high studentized contrast indicating high correlation of this unit with Cu mineralization in the modelling space. The granodiorite units are

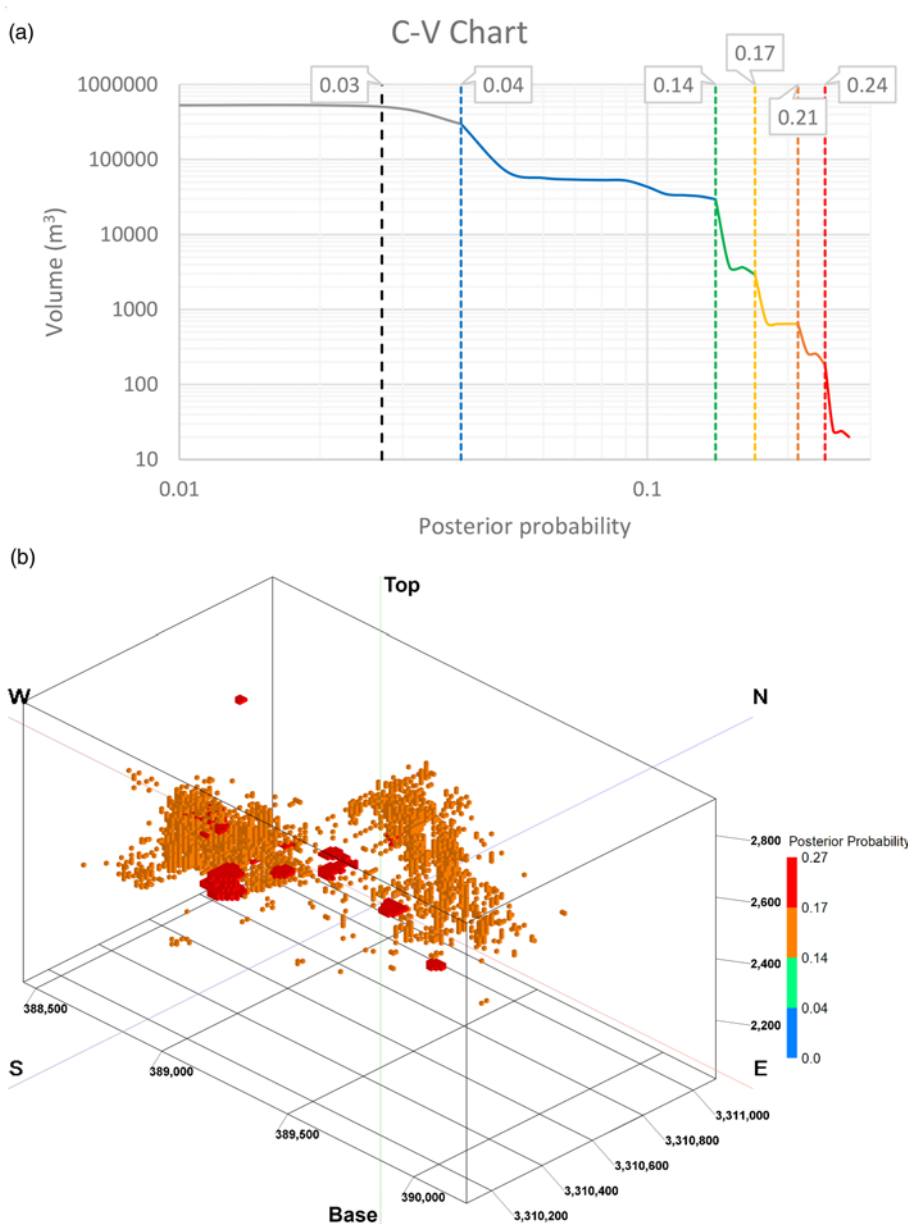


Fig. 13. (a) C-V chart of the posterior probability of Cu mineralization in the modelling space; the prior probability drawn using black dashed line. (b) Classified anomalous voxels based on the thresholds determined by the C-V chart.

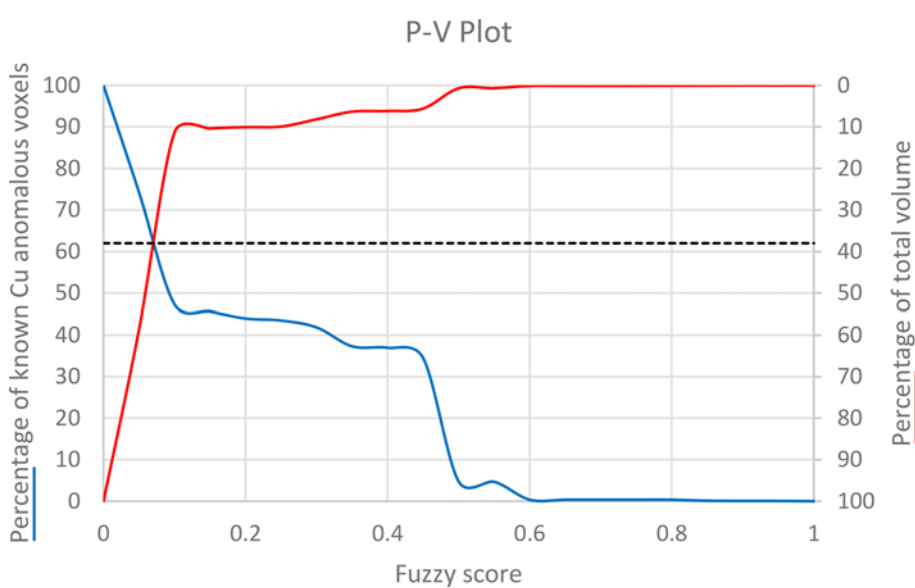


Fig. 14. P-V plot of the posterior probability model.

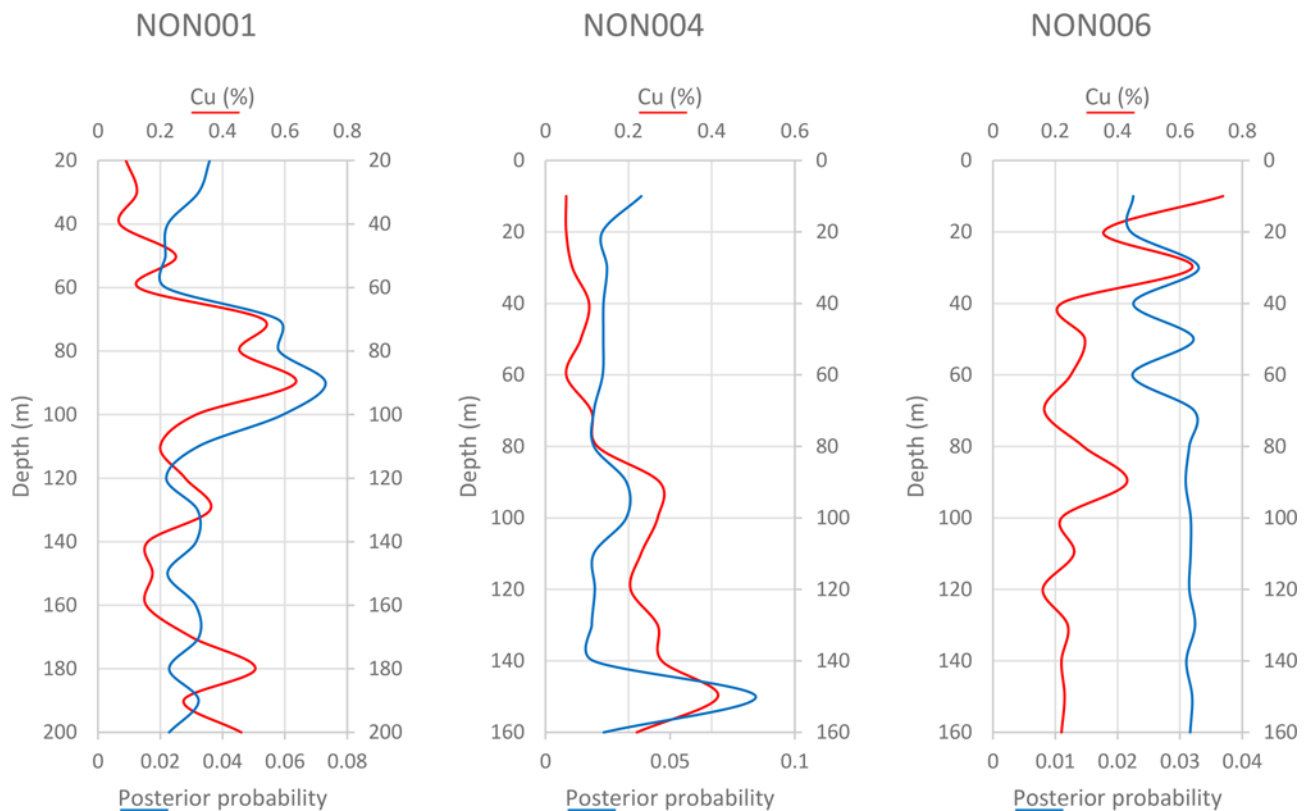


Fig. 15. Variations of the posterior probability and Cu concentration along three of the test boreholes.

in the second place in terms of the highest contrast and volume percentage showing a high studentized contrast. Most of the modelling space is occupied by andesite (Fig. 10a) which shows a contrast near zero, but a high studentized contrast. According to Figure 9a, high-grade Cu concentration is associated with stockwork veins mainly hosted by andesite which can be due to the high porosity and permeability of this lithology type caused by fractures. These probable fractures provide a path for hydrothermal fluids to the ground surface. In Figure 9a, the cross-section B-B' appears to show a vertical pipe hosted by andesite and characterized by elevated Cu concentration where the section A-A' crosses section B-B'.

Among the different types of alteration in the study area, carbonatized, epidotized, potassic and silicified units show positive contrast and studentized contrast (Table 2). According to the results, epidotized and silicified units show the highest contrast, respectively. The epidotized units occupy a very small portion of the modelling space and the results are not reliable. It is noteworthy that the contrast of silica alteration is much higher than the epidotized units. This is compatible with the metallogenetic model of the mineralization in the study area, because Cu mineralization is mostly observed along the silicified veins. The potassic alteration which occupies most of the modelling space, shows a very high studentized contrast, but a low contrast indicating the low uncertainty associated with this unit. The carbonatized units show a relatively high studentized contrast, but a low contrast. According to the metallogenetic model, malachite and azurite are considered as the main ore minerals which are related to the carbonatized units.

According to Figure 6c, the rocks located in the modelling space originate from five different sources, and only volcanic units show a positive contrast. This unit which occupies a significant portion of the modelling space, shows a low contrast and a high studentized contrast. We used surficial structural data for creating a 3D model of the fault surfaces due to lack of structural information in the drilling data. In addition to the fault surfaces which were converted into the

fault blocks, two different buffer zones in a radius of 25 and 50 m were created surrounding the fault blocks. All the structural models show a negative contrast and were removed from the modelling process. This confirms the field observations implying that the Cu-bearing mineralization zones in the study area, are mainly associated with azurite and malachite stockwork veins and less associated with the faults.

Besides the qualitative geological data, we used the quantitative geochemical data consisting of the concentration values of three elements including Fe, Mo and Zn. These elements are known as the key indicators of Cu mineralization in the study area. We used factor analysis to reduce the dimension of the geochemical data and to maximize the conditional independence. As explained in the Weights of evidence modelling section, to minimize the loss of information in processing continuous models, we determined the fuzzy weight of each class in the two geochemical factors. According to Tables 3 and 4, the highest contrast and studentized contrast values belong to the large values of the first factor. Based on the results, there is no linear relationship between contrast and fuzzy weight in continuous models, and a high contrast does not necessarily yield a high fuzzy weight. On the other hand, we see a clear inverse relationship between variance of contrast and studentized contrast.

Eventually, we created a posterior probability model for visualizing Cu mineralization potential in the target modelling space. Based on the results, where there are a low number of boreholes, the total variance shows a high value which gives a high uncertainty. Therefore, we removed the voxels associated with a high uncertainty. The intersection point in the P-V plot of the posterior probability model shows that more than 60% of the anomalous voxels in the interpolated model of Cu concentration have been predicted in less than 40% of the total modelling space. The contribution of uncertainty in creating the posterior probability model can lead to a higher prediction rate. Moreover, we compared the posterior probability and Cu concentration values along the test

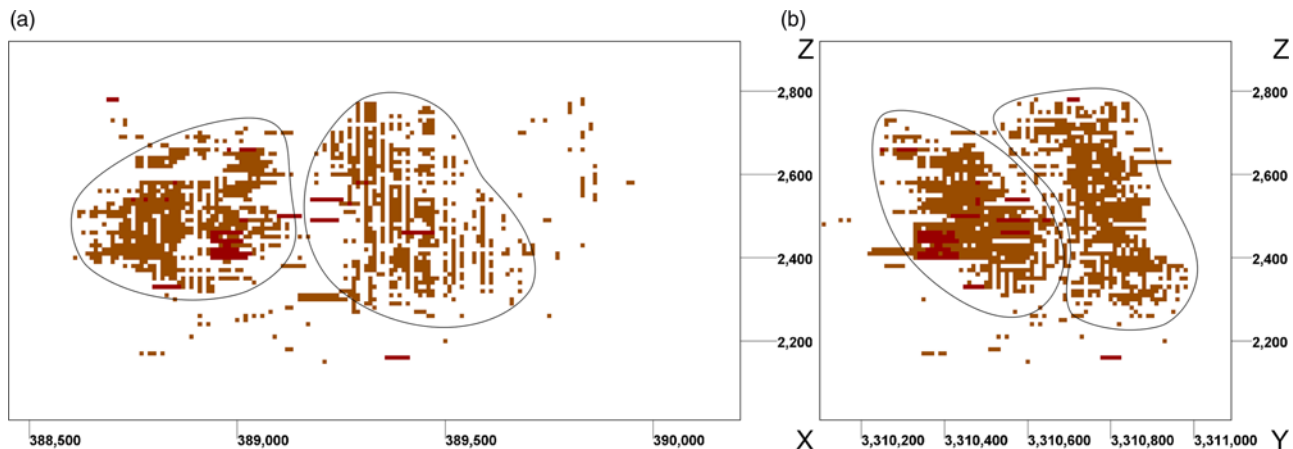


Fig. 16. Side views of the posterior probability model to the (a) north, and (b) west.

boreholes and determined the Pearson correlation coefficient for each. Based on the results, the coefficient is above 0.5 where the test borehole is surrounded by other boreholes at a short distance, and the boreholes located at the edge of the modelling space show a weak correlation. The ore body and the variation of Cu mineralization with depth are obvious and outlined in Figure 16. According to this figure, the ore body is divided into two parts. One is located in SW of the modelling space and the other is located in NE. A significant volume of the ore body is located between the elevation levels of 2400 to 2600 m.

We implemented 3D WofE modelling using Python scripts and released them as open-source software (see [supplementary files](#)). The scripts are simple and easy to understand for a user with basic knowledge of programming and can be extended for other types of problems which can be considered as the main advantages.

Conclusions

In this study, we created a mineral prospectivity model based on 3D weights of evidence by integration of qualitative geological and quantitative geochemical borehole data located on a porphyry Cu deposit in SE Iran. To minimize the loss of information, we determined the ordinary and fuzzy weights of evidence for discrete and continuous evidential models, respectively. The integration of various input evidential models led to the posterior probability model and the C-V fractal models were used to find suitable thresholds for classifying and separating anomalous voxels. The voxels with high total variance, which represents the uncertainty associated with each voxel, were removed from the posterior model to make it more reliable. The posterior probability model shows an acceptable prediction rate based on the P-V plot and the high correlation observed between real data and posterior probability in the test boreholes. The results show the efficiency of our framework in constructing a geometric model of a specific ore deposit concealed in depth. The proposed framework helps in determining the key factors which control the mineralization in the modelling space, identifying potential mineralization, and improving the perception of ore genesis.

Among the lithological units, diorite dykes, andesite and granodiorite show a high correlation with Cu mineralization in the modelling space. Moreover, silica, carbonate and potassic alteration types are strongly associated with Cu mineralization. According to the results of mineral prospectivity modelling, it is concluded that Cu mineralization is mainly associated with stockwork veins which confirms the field observations. The Cu mineralization is identified in two separate bodies located in depth and covered by a thin layer of regolith.

The hybrid application of ordinary and fuzzy weights of evidence yields a promising result for the future studies. The 3D mineral prospectivity modelling based on the weights of evidence is highly dependent on the primary model created using the concentration values of a specific target element. In the future, we aim to use geostatistical methods to create a more reliable model to consider as the primary target ore body, since we can provide an uncertainty model alongside the model yielded by the interpolation process. In addition, we can decrease the uncertainty and increase the prediction rate in our posterior probability model by adding other exploration data such as geochemical and geophysical models and creating more input evidential models compatible to the metallogenetic model of the study area.

Acknowledgement The authors would like to thank Prof. S. A. Wood for handling this paper and constructive comments. This paper benefited significantly from detailed comments of Dr. G. Bonham-Carter. We acknowledge National Iranian Copper Industries Company for providing the data and consultancy.

Funding This research received no specific grant from any funding agency in the public, commercial, or not-for-profit sectors.

Author contributions EF: methodology (lead), software (lead), writing - original draft (lead); AH: supervision (lead); TE: supervision (lead); AB: supervision (supporting); RC: supervision (supporting), writing - review & editing (supporting).

Data availability statement The datasets generated during and/or analysed during the current study are available in the GitHub repository, https://github.com/intelligent-exploration/3D_WoFE.

Scientific editing by Scott Wood

References

- Abedi, M., Gholami, A. and Norouzi, G.H. 2014. 3D inversion of magnetic data seeking sharp boundaries: A case study for a porphyry copper deposit from Now Chun in central Iran. *Near Surface Geophysics*, **12**, 657–666, <https://doi.org/10.3997/1873-0604.2014022>
- Afzal, P., Alghalandis, Y.F., Khakzad, A., Moarefvand, P. and Omran, N.R. 2011. Delineation of mineralization zones in porphyry Cu deposits by fractal concentration-volume modeling. *Journal of Geochemical Exploration*, **108**, 220–232, <https://doi.org/10.1016/j.gexplo.2011.03.005>
- Agterberg, F.P., Bonham-Carter, G.F. and Wright, D.F. 1990. Statistical Pattern Integration for Mineral Exploration. In: Gaal, G. and Merriam, D.F. (eds) *Computer Applications in Resource Estimation*. Computers and Geology, 1–21. <https://doi.org/10.1016/B978-0-08-037245-7.50006-8>.
- ArcGIS Desktop. 2019. ESRI. Environmental Systems Research Institute, Redlands, CA, <https://www.esri.com/en-us/arcgis/about-arcgis/overview>
- Berberian, F. and Berberian, M. 1981. Tectono-Plutonic Episodes in Iran. In: Gupta, H.K. and Delany, F.M. (eds) *Zagros Hindu Kush Himalaya*

- Geodynamic Evolution*, American Geophysical Union, Washington, D.C., USA, 5–32, <https://doi.org/10.1029/GD003p0005>
- Berger, B.R., Ayuso, R.A., Wynn, J.C. and Seal, R.R. 2008. *Preliminary Model of Porphyry Copper Deposits*, U.S. Geological Survey Open-File Report 2008-1321, Reston, VA, USA, <https://doi.org/10.1127/0077-7749/2011/0172>
- Bonham-Carter, G.F. 1994. *Geographic Information Systems for Geoscientists: Modeling with GIS*, Pergamon, Oxford, UK.
- Bonham-Carter, G.F., Agterberg, F.P. and Wright, D.F. 1989. Weights of evidence modelling: A new approach to mapping mineral potential. In: Agterberg, F.P. and Bonham-Carter, G.F. (eds) *Statistical Applications in the Earth Sciences*, Geological Survey of Canada, Ottawa, Canada, 171–183.
- Brown, W.M., Gedeon, T.D., Groves, D.I. and Barnes, R.G. 2000. Artificial neural networks: A new method for mineral prospectivity mapping. *Australian Journal of Earth Sciences*, **47**, 757–770, <https://doi.org/10.1046/j.1440-0952.2000.00807.x>
- Carranza, E.J.M. 2004. Weights of evidence modeling of mineral potential: A case study using small number of prospects, Abra, Philippines. *Natural Resources Research*, **13**, 173–187, <https://doi.org/10.1023/B:NARR.0000046919.87758.f5>
- Carranza, E.J.M. 2009. Controls on mineral deposit occurrence inferred from analysis of their spatial pattern and spatial association with geological features. *Ore Geology Reviews*, **35**, 383–400, <https://doi.org/10.1016/j.oregeorev.2009.01.001>
- Carranza, E.J.M. 2011. Analysis and mapping of geochemical anomalies using logratio-transformed stream sediment data with censored values. *Journal of Geochemical Exploration*, **110**, 167–185, <https://doi.org/10.1016/j.gexplo.2011.05.007>
- Carranza, E.J.M. and Laborte, A.G. 2015. Random forest predictive modeling of mineral prospectivity with small number of prospects and data with missing values in Abra (Philippines). *Computers & Geosciences*, **74**, 60–70, <https://doi.org/10.1016/j.cageo.2014.10.004>
- Carranza, E.J.M. and Sadeghi, M. 2010. Predictive mapping of prospectivity and quantitative estimation of undiscovered VMS deposits in Skellefte district (Sweden). *Ore Geology Reviews*, **38**, 219–241, <https://doi.org/10.1016/j.oregeorev.2010.02.003>
- Carranza, E.J.M., Woldai, T. and Chikambwe, E.M. 2005. Application of data-driven evidential belief functions to prospectivity mapping for aquamarine-bearing pegmatites, Lundazi district, Zambia. *Natural Resources Research*, **14**, 47–63, <https://doi.org/10.1007/s11053-005-4678-9>
- Carranza, E.J.M., van Ruitenberg, F.J.A., Hecker, C., van der Meijde, M. and van der Meer, F.D. 2008. Knowledge-guided data-driven evidential belief modeling of mineral prospectivity in Cabo de Gata, SE Spain. *International Journal of Applied Earth Observation and Geoinformation*, **10**, 374–387, <https://doi.org/10.1016/j.jag.2008.02.008>
- Chen, Y. and Wu, W. 2017. Mapping mineral prospectivity using an extreme learning machine regression. *Ore Geology Reviews*, **80**, 200–213, <https://doi.org/10.1016/j.oregeorev.2016.06.033>
- Cheng, Q. and Agterberg, F.P. 1999. Fuzzy weights of evidence method and its application in mineral potential mapping. *Natural Resources Research*, **8**, 27–35, <https://doi.org/10.1023/A:1021677510649>
- Comas-Cufí, M. and Thió-Henestrosa, S. 2011. CoDaPack 2.0: A stand-alone, multi-platform compositional software. In: Egozcue, J.J., Tolosana-Delgado, R. and Ortego, M.I. (eds) *CoDaWork'11: 4th International Workshop on Compositional Data Analysis*, Sant Feliu de Guíxols, Spain.
- Fallara, F., Legault, M. and Rabreau, O. 2006. 3-D integrated geological modeling in the Abitibi Subprovince (Québec, Canada): Techniques and applications. *Exploration and Mining Geology*, **15**, 27–43, <https://doi.org/10.2113/gsem.15.1-2.27>
- Farahbakhsh, E., Chandra, R., Olieroor, H.K.H., Scalzo, R., Clark, C., Reddy, S.M. and Müller, R.D. 2019a. Computer vision-based framework for extracting tectonic lineaments from optical remote sensing data. *International Journal of Remote Sensing*, **41**, 1760–1787, <https://doi.org/10.1080/01431161.2019.1674462>
- Farahbakhsh, E., Chandra, R., Eslamkish, T. and Müller, R.D. 2019b. Modeling geochemical anomalies of stream sediment data through a weighted drainage catchment basin method for detecting porphyry Cu-Au mineralization. *Journal of Geochemical Exploration*, **204**, 12–32, <https://doi.org/10.1016/j.gexplo.2019.05.003>
- Filzmoser, P., Hron, K. and Reimann, C. 2009. Univariate statistical analysis of environmental (compositional) data: Problems and possibilities. *Science of the Total Environment*, **407**, 6100–6108, <https://doi.org/10.1016/j.scitotenv.2009.08.008>
- Houlding, S. 1994. *3D Geoscience Modeling: Computer Techniques for Geological Characterization*, Springer, Berlin, Germany.
- IBM Corp 2019. *IBM SPSS Statistics for Windows, Version 26.0*. IBM Corp. <https://www.ibm.com/products/spss-statistics>.
- Jessell, M., Aillères, L. *et al.* 2014. Next Generation Three-Dimensional Geologic Modeling and Inversion. In: Kelley, K.D. and Golden, H.C. (eds) *Building Exploration Capability for the 21st Century*, Society of Economic Geologists, Littleton, CO, USA, 261–272, <https://doi.org/10.5382/SP.18.13>
- Joly, A., Porwal, A. and McCuaig, T.C. 2012. Exploration targeting for orogenic gold deposits in the Granites-Tanami Orogen: Mineral system analysis, targeting model and prospectivity analysis. *Ore Geology Reviews*, **48**, 349–383, <https://doi.org/10.1016/j.oregeorev.2012.05.004>
- Knox-Robinson, C.M. 2000. Vectorial fuzzy logic: A novel technique for enhanced mineral prospectivity mapping, with reference to the orogenic gold mineralisation potential of the Kalgoorlie Terrane, Western Australia. *Australian Journal of Earth Sciences*, **47**, 929–941, <https://doi.org/10.1046/j.1440-0952.2000.00816.x>
- Kreuzer, O.P., Miller, A.V.M. *et al.* 2015. Comparing prospectivity modelling results and past exploration data: A case study of porphyry Cu-Au mineral systems in the Macquarie Arc, Lachlan Fold Belt, New South Wales. *Ore Geology Reviews*, **71**, 516–544, <https://doi.org/10.1016/j.oregeorev.2014.09.001>
- Li, X., Yuan, F. *et al.* 2015. Three-dimensional mineral prospectivity modeling for targeting of concealed mineralization within the Zhonggu iron orefield, Ningwu basin, China. *Ore Geology Reviews*, **71**, 633–654, <https://doi.org/10.1016/j.oregeorev.2015.06.001>
- Li, N., Song, X., Xiao, K., Li, S., Li, C. and Wang, K. 2018. Part II: A demonstration of integrating multiple-scale 3D modelling into GIS-based prospectivity analysis: A case study of the Huayuan-Malichang district, China. *Ore Geology Reviews*, **95**, 292–305, <https://doi.org/10.1016/j.oregeorev.2018.02.034>
- Lindsay, M.D., Aillères, L., Jessell, M.W., de Kemp, E.A. and Betts, P.G. 2012. Locating and quantifying geological uncertainty in three-dimensional models: Analysis of the Gippsland basin, Southeastern Australia. *Tectonophysics*, **546–547**, 10–27, <https://doi.org/10.1016/j.tecto.2012.04.007>
- Liu, L., Li, J., Zhou, R. and Sun, T. 2016. 3D modeling of the porphyry-related Dawangding gold deposit in south China: Implications for ore genesis and resources evaluation. *Journal of Geochemical Exploration*, **164**, 164–185, <https://doi.org/10.1016/j.gexplo.2015.11.002>
- Lowell, J.D. and Gilbert, J.M. 1970. Lateral and vertical alteration-mineralization zoning in porphyry ore deposits. *Economic Geology*, **65**, 373–408, <https://doi.org/10.2113/gsecongeo.65.4.373>
- Manap, M.A., Sulaiman, W.N.A., Ramli, M.F., Pradhan, B. and Surip, N. 2013. A knowledge-driven GIS modeling technique for groundwater potential mapping at the Upper Langat Basin, Malaysia. *Arabian Journal of Geosciences*, **6**, 1621–1637, <https://doi.org/10.1007/s12517-011-0469-2>
- Mao, X., Ren, J. *et al.* 2019. Three-dimensional prospectivity modeling of the Jiaoja-type gold deposit, Jiaodong Peninsula, Eastern China: A case study of the Dayingzhuang deposit. *Journal of Geochemical Exploration*, **203**, 27–44, <https://doi.org/10.1016/j.gexplo.2019.04.002>
- Meng, L. 1997. Metallogenetic model of the copper deposit. *Science in China Series D: Earth Sciences*, **40**, 225–231, <https://doi.org/10.1007/BF02877529>
- Mudd, G.M. and Jowitt, S.M. 2018. Growing global copper resources, reserves and production: Discovery is not the only control on supply. *Economic Geology*, **113**, 1235–1267, <https://doi.org/10.5382/econgeo.2018.4590>
- Mudd, G.M., Weng, Z. and Jowitt, S.M. 2013. A detailed assessment of global Cu resource trends and endowments. *Economic Geology*, **108**, 1163–1183, <https://doi.org/10.2113/econgeo.108.5.1163>
- Nielsen, S.H.H., Cunningham, F., Hay, R., Partington, G. and Stokes, M. 2015. 3D prospectivity modelling of orogenic gold in the Marymia Inlier, Western Australia. *Ore Geology Reviews*, **71**, 578–591, <https://doi.org/10.1016/j.oregeorev.2015.02.001>
- Nielsen, S.H.H., Partington, G.A., Franey, D. and Dwight, T. 2019. 3D mineral potential modelling of gold distribution at the Tampia gold deposit. *Ore Geology Reviews*, **109**, 276–289, <https://doi.org/10.1016/j.oregeorev.2019.04.012>
- Olieroor, H.K.H., Scalzo, R. *et al.* 2020. Bayesian geological and geophysical data fusion for the construction and uncertainty quantification of 3D geological models. *Geoscience Frontiers*, <https://doi.org/10.1016/j.gsf.2020.04.015>
- Omraní, J., Agard, P., Whitechurch, H., Benoit, M., Prouteau, G. and Jolivet, L. 2008. Arc-magmaism and subduction history beneath the Zagros Mountains, Iran: A new report of adakites and geodynamic consequences. *Lithos*, **106**, 380–398, <https://doi.org/10.1016/j.lithos.2008.09.008>
- Payne, C.E., Cunningham, F., Peters, K.J., Nielsen, S., Puccioni, E., Wildman, C. and Partington, G.A. 2015. From 2D to 3D: Prospectivity modelling in the Taupo volcanic zone, New Zealand. *Ore Geology Reviews*, **71**, 558–577, <https://doi.org/10.1016/j.oregeorev.2014.11.013>
- Pazand, K. and Hezarkhani, A. 2014. The use of the weights-of-evidence modeling technique to predictive porphyry Cu potential mapping in Ahar-Arasbaran zone, Iran. *Arabian Journal of Geosciences*, **7**, 4191–4201, <https://doi.org/10.1007/s12517-013-0983-5>
- Pearson, K. 1895. Notes on regression and inheritance in the case of two parents. *Proceedings of the Royal Society of London*, 240–242.
- Porwal, A., Carranza, E.J.M. and Hale, M. 2003. Knowledge-driven and data-driven fuzzy models for predictive mineral potential mapping. *Natural Resources Research*, **12**, 1–25, <https://doi.org/10.1023/A:1022693220894>
- Porwal, A., González-Alvarez, I., Markwitz, V., McCuaig, T.C. and Mamuse, A. 2010. Weights-of-evidence and logistic regression modeling of magmatic nickel sulfide prospectivity in the Yilgarn craton, Western Australia. *Ore Geology Reviews*, **38**, 184–196, <https://doi.org/10.1016/j.oregeorev.2010.04.002>
- QGIS Development Team 2019. QGIS Geographic Information System. *Open Source Geospatial Foundation Project*.
- RockWorks17 2019a. *Software (Revision 2019.7.30)*. RockWare, Inc., Golden, CO, USA, <https://www.rockware.com/product/rockworks/>

- RockWorks17 2019b. *Software Help Files (Revision 2019.7.30)*. RockWare, Inc., Golden, CO, USA, <https://help.rockware.com/rockworks17/WebHelp/introduction.htm>
- Rodriguez-Galiano, V., Sanchez-Castillo, M., Chica-Olmo, M. and Chica-Rivas, M. 2015. Machine learning predictive models for mineral prospectivity: An evaluation of neural networks, random forest, regression trees and support vector machines. *Ore Geology Reviews*, **71**, 804–818, <https://doi.org/10.1016/j.oregeorev.2015.01.001>
- Scalzo, R., Kohn, D., Olieroock, H., Houseman, G., Chandra, R., Girolami, M. and Cripps, S. 2019. Efficiency and robustness in Monte Carlo sampling for 3-D geophysical inversions with Obsidian v0.1.2: Setting up for success. *Geoscientific Model Development*, **12**, 2941–2960, <https://doi.org/10.5194/gmd-12-2941-2019>
- Schedde, R. 2013. Long term outlook for the global exploration industry—gloom or boom. In: Geological Society of South Africa GeoForum Conference.
- Shirmard, H., Farahbakhsh, E., Pour, A.B., Muslim, A.M., Müller, R.D. and Chandra, R. 2020. Integration of selective dimensionality reduction techniques for mineral exploration using ASTER satellite data. *Remote Sensing*, **12**, 1261, <https://doi.org/10.3390/rs12081261>
- Sillitoe, R.H. 2010. Porphyry copper systems. *Economic Geology*, **105**, 3–41, <https://doi.org/10.2113/gsecongeo.105.1.3>
- Sun, T., Chen, F., Zhong, L., Liu, W. and Wang, Y. 2019. GIS-based mineral prospectivity mapping using machine learning methods: A case study from Tongling ore district, eastern China. *Ore Geology Reviews*, **109**, 26–49, <https://doi.org/10.1016/j.oregeorev.2019.04.003>
- Wang, G. and Huang, L. 2012. 3D geological modeling for mineral resource assessment of the Tongshan Cu deposit, Heilongjiang Province, China. *Geoscience Frontiers*, **3**, 483–491, <https://doi.org/10.1016/j.gsf.2011.12.012>
- Waterman, G.C. and Hamilton, R.L. 1975. The Sar Cheshmeh porphyry copper deposit. *Economic Geology*, **70**, 568–576, <https://doi.org/10.2113/gsecongeo.70.3.568>
- Xiao, F., Chen, J., Agterberg, F. and Wang, C. 2014. Element behavior analysis and its implications for geochemical anomaly identification: A case study for porphyry Cu-Mo deposits in Eastern Tianshan, China. *Journal of Geochemical Exploration*, **145**, 1–11, <https://doi.org/10.1016/j.gexplo.2014.04.008>
- Xiao, K., Li, N., Porwal, A., Holden, E.J., Bagas, L. and Lu, Y. 2015. GIS-based 3D prospectivity mapping: A case study of Jiamal copper-polymetallic deposit in Tibet, China. *Ore Geology Reviews*, **71**, 611–632, <https://doi.org/10.1016/j.oregeorev.2015.03.001>
- Xiong, Y. and Zuo, R. 2018. GIS-based rare events logistic regression for mineral prospectivity mapping. *Computers & Geosciences*, **111**, 18–25, <https://doi.org/10.1016/j.cageo.2017.10.005>
- Yousefi, M. and Carranza, E.J.M. 2015. Fuzzification of continuous-value spatial evidence for mineral prospectivity mapping. *Computers and Geosciences*, **74**, 97–109, <https://doi.org/10.1016/j.cageo.2014.10.014>
- Yuan, F., Li, X., Zhang, M., Jowitt, S.M., Jia, C., Zheng, T. and Zhou, T. 2014. Three-dimensional weights of evidence-based prospectivity modeling: A case study of the Baixiangshan mining area, Ningwu Basin, Middle and Lower Yangtze Metallogenic Belt, China. *Journal of Geochemical Exploration*, **145**, 82–97, <https://doi.org/10.1016/j.gexplo.2014.05.012>
- Zeghouane, H., Allek, K. and Kesraoui, M. 2016. GIS-based weights of evidence modeling applied to mineral prospectivity mapping of Sn-W and rare metals in Laouini area, Central Hoggar, Algeria. *Arabian Journal of Geosciences*, **9**, 373, <https://doi.org/10.1007/s12517-015-2188-6>
- Zuo, R. 2011. Identifying geochemical anomalies associated with Cu and Pb-Zn skarn mineralization using principal component analysis and spectrum-area fractal modeling in the Gangdese Belt, Tibet (China). *Journal of Geochemical Exploration*, **111**, 13–22, <https://doi.org/10.1016/j.gexplo.2011.06.012>
- Zuo, R., John, E. and Carranza, E.J.M. 2011. Support vector machine: A tool for mapping mineral prospectivity. *Computers & Geosciences*, **37**, 1967–1975, <https://doi.org/10.1016/j.cageo.2010.09.014>
- Zuo, R., Carranza, E.J.M. and Wang, J. 2016. Spatial analysis and visualization of exploration geochemical data. *Earth-Science Reviews*, **158**, 9–18, <https://doi.org/10.1016/j.earscirev.2016.04.006>